IV ECCOMAS Thematic Conference on the Mechanical Response of Composites
Composites 2013
A. Suleman, P. Camanho, et al. (Editors)
© IDMEC 2013

Investigation of Static and Dynamic Failure Behaviour of Composite T-Joints

S. Heimbs[a,1], A. Mierzwa[a], T. Duwensee[a], C. Breu[a], A.C. Nogueira[a], M. May[b], C. Less[c], J. Wolfrum[d]

[a]EADS, Innovation Works, 81663 Munich, Germany
sebastian.heimbs@eads.net

[b]Fraunhofer Institute for High-Speed Dynamics (EMI), Eckerstraße 4, 79104 Freiburg, Germany
michael.may@emi.fraunhofer.de

[c]IABG mbH, Einsteinstraße 20, 85521 Ottobrunn, Germany
less@iabg.de

[d]Wehrwissenschaftliches Institut für Werk- und Betriebsstoffe (WIWeB), Institutsweg 1, 85435 Erding, Germany
johanneswolfrum@bundeswehr.org

ABSTRACT

An experimental and numerical study of the failure behaviour of composite T-joints under quasi-static and high-rate dynamic loads is presented, including the investigation of different joint designs to increase damage tolerance and failure resistance.

Three different T-joint designs using the same carbon fibre composite base material were used in this study. Two pure composite solutions and a hybrid design with arrow head-shaped metallic reinforcement pins in the through-thickness direction are presented. Specimen manufacturing and testing is described in detail. The test campaigns covering 0° T-pull and 30° T-bending tests were conducted under quasi-static and high-rate dynamic conditions in order to assess potential strain rate effects. The hybrid solution with the pin-reinforcement showed significantly increased post-damage load levels and energy absorption with the pins being pulled out of the laminate under large global deformations. The utilisation of a modern toughened epoxy resin in comparison to a conventional untoughened resin also showed significant improvements.

In addition to the experimental test campaign, numerical simulations with the explicit Finite Element code LS-DYNA were conducted on micro, meso and macro level. The models were validated against the test results and applied to a ballistic impact simulation of a composite fuel tank structure under hydrodynamic ram loading.

1. INTRODUCTION

Joints between members or surfaces can be the weak link of loaded structures and joint failure can, in the worst case, lead to global structural failure.

The focus of this research study is on composite T-joints as a typical connection to be found in aircraft wing structures and wing integral tanks. Fuel-filled wing tanks may be susceptible to a load case that is called hydrodynamic ram (HRAM), which is the result of a ballistic impact and projectile penetration through the outer skin into the fuel. The shock front that develops and propagates inside

[1] Corresponding author

the fluid may lead to very high pressures acting on the tank structure with potential structural damage [1-10]. Typical locations for damage are the structural T-joint connections between skin and spar. This load case may occur in military combat or observation aircraft resulting from hostile attacks or in civil aircraft as a result of turbine blade release or other foreign object impact (see Concorde accident [11]).

The aim of the current study is to characterise the failure behaviour of such composite T-joints both experimentally and numerically and to investigate design alternatives aiming at increased damage tolerance and failure resistance. For this purpose, the mechanical behaviour both under quasi-static and dynamic loads is assessed. Although numerous publications focussing on quasi-static T-joint testing can be found [12-20], only very few researchers have studied the high-rate failure behaviour of such composite joints. In [21] and [22] dynamic T-pull tests were performed investigating different composite T-joint designs with minor strain rate effects occurring in unreinforced samples and a 25%-60% increased failure load being observed in samples reinforced by stitching. Even higher strain rates were accomplished in the RamGun T-pull tests in [23-25], which aim at a realistic hydrodynamic ram loading under a pressure shock wave in a fluid chamber.

In addition to the experimental test campaign, numerical simulations with the explicit finite element (FE) code LS-DYNA were conducted in order to be able to investigate further geometrical and boundary influences on the structural behaviour. Several numerical studies of composite T-joint failure have been conducted in past publications [13, 26-34], almost entirely using very detailed models in implicit FE codes in order to capture stress concentrations and mechanical effects on micro-scale level. However, for hydrodynamic ram analyses, much coarser and more efficient T-joint models are needed in explicit simulation environments that are still supposed to capture realistic failure loads. Therefore, different modelling approaches on different scales (micro, meso and macro) with increasing degree of simplification are presented here and compared to the experimental test results. Finally, the application of the T-joint models to hydrodynamic ram simulations in fuel-filled composite fuel tanks under ballistic impact is shortly addressed.

2. DESIGN CONCEPTS

The aim within this project was to investigate the failure behaviour of three different composite T-joint designs by experiment and simulation. The first one (baseline, D1) should be a state-of-the-art design that can be found in various aircraft structures and that can act as a reference. It consists of a flange, which splits into two distinct flange feet that are connected to the skin by co-curing (Fig. 1a).

The second design D2 is a slight modification or improvement of design D1. The flange feet have no specific edge but continue to the next flange, forming an integral part of the skin (Fig. 1b). Although this design is not expected to increase the damage initiation load, it is intended to enable higher energy absorption under tensile loads by a higher delamination surface and to enable structural integrity and leak tightness in a fuel tank application.

The third design D3 includes a z-reinforcement to increase the connection between flange feet and skin. Numerous past studies have shown that z-reinforcements in composite T-joints can significantly increase the maximum load carrying capability of the joint. Early studies investigated stitching or tufting [21, 35-43] as reinforcement methods with considerable results, while in younger days the focus seems to be on z-pinning [13, 15, 43-46]. All these methods typically use polymeric yarns or carbon fibres for the z-reinforcement. A different promising alternative can be the use of metallic reinforcement concepts in a hybrid joint, making use of the metallic plasticity, which is especially beneficial for high energy absorption targets. Such hybrid joints using metallic sheets with reinforcement pins connecting carbon fibre laminates were investigated in different recent studies with the metallic pins made of titanium or steel being produced either by additive layer manufacturing (ALM) [47, 48], welding [49] or metal forming [50, 51]. Pins with arrow-shaped heads were

© IDMEC 2013

investigated in [47], leading to a strong mechanical interlocking effect within the composite laminate. For this reason, the metal pin-reinforcement approach was also selected to be studied here, making use of the RHEA (redundant high efficiency assembly) technique based on formed, spiked metal sheet inserts described in [50, 52]. The basic idea is to use a thin metallic sheet, in this case a 0.4 mm DC4 steel sheet, where the pin geometry is laser-cut and bent on a special bending machine in order to obtain a reinforcement sheet with pins on both sides (Fig. 2). This sheet is intended to be placed between two laminates, in this case between flange and skin. On the one hand, the pins are supposed to be as thin and few as possible in order to minimise fibre ondulation and disturbance when being inserted into the laminate. On the other hand, the pins need to have a certain minimum thickness and quantity in order to enable high strength and beneficial reinforcement effects. A compromise was needed to be found here, which led to the design shown in Fig. 2 with arrow-shaped pins on both sides.

Further design studies related to the design or radius of the fillet in the centre of the specimens (as in [34, 53, 54]) were not part of the experimental programme and were to be investigated numerically.

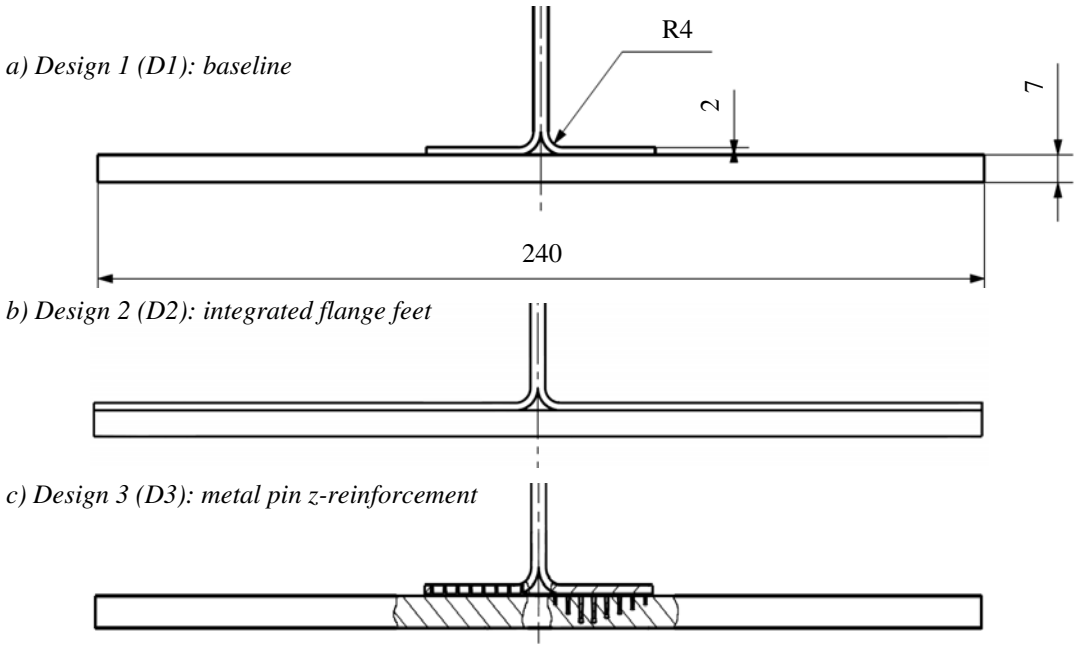

Figure 1: Three composite T-joint design concepts investigated in this study (dimensions in mm)

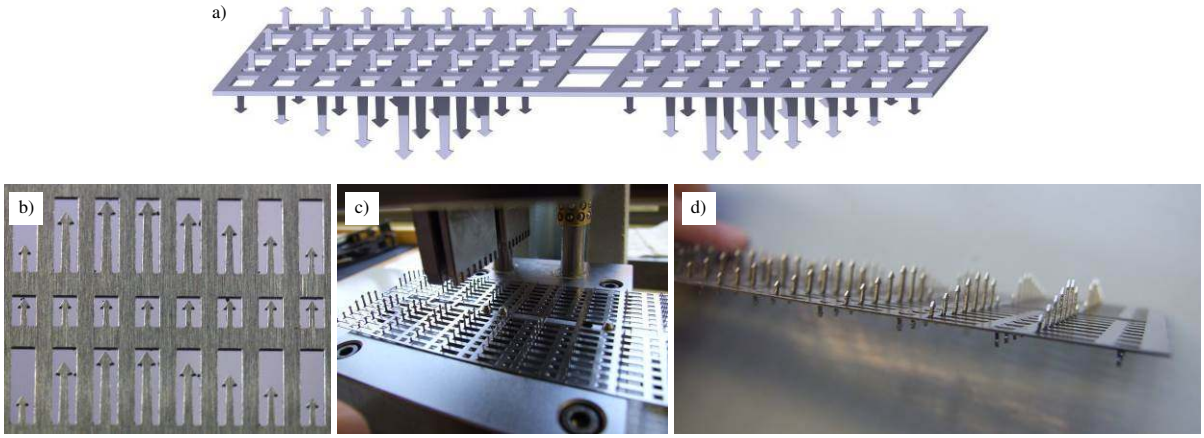

Figure 2: Metal pin reinforcement of design D3: a) CAD design, b) laser-cut steel sheet, c) bending of pins, d) final pin-reinforcement sheet

3. MATERIALS AND MANUFACTURING

All three composite T-joint concepts are using the same base material, which is a Saertex carbon fibre non-crimped fabric (NCF) with Tenax HTS fibres in biaxial, triaxial and quadraxial configuration. The baseline resin was Hexcel HexFlow® RTM6, a standard untoughened aerospace grade 180°C epoxy resin system. In order to investigate the influence of the resin system on the structural performance, half of the D2 T-joint samples were manufactured using Cytec Prism® EP2400 resin, a state-of-the-art toughened 180°C epoxy system. The T-joint flange had a uniform thickness of 4 mm with a stacking sequence of $[+45°/0°/-45°/+45°/-45°/+45°/0°/-45°]_S$ for the D1 and D3 specimens. The skin of D1 and D3 had a stacking sequence of $[0°/+45°/90°/-45°/0°/-45°/90°/+45°/0°/+45°/90°/-45°/0°/90°]_S$ with a thickness of 7 mm. The flange laminate of D2 was slightly different with less 45° plies $[0°/+45°/90°/-45°/0°/-45°/90°/+45°]_S$ as it was supposed to extend completely onto the skin, which had a final thickness of 9 mm.

The basic toolings for the T-joint sample manufacturing were two L-shaped strand-casted and milled steel profiles with a length of 1270 mm, allowing manufacturing of eight T-joint specimens with one shot. Firstly, the flange plies were stacked, placed between the toolings and cut according to the milled groove for the flange feet (Fig. 3a). Afterwards, a braided carbon fibre fillet supplied by Eurocarbon was put in the middle between the two halves of the folded flange plies. For the D3 specimens with z-reinforcement, the sand-blasted and acetone-cleaned metallic pin sheets were then pushed into the dry fabric with a special tool (Fig. 3b). Then, the skin plies were placed on top (Fig. 3c). After turning the tooling around, the vacuum-assisted resin infusion process (VAP) was prepared by wrapping the assembly in the specific fabrics, membranes and vacuum bagging films (Fig. 3d). The vacuum valves were installed (Fig. 3e) and the pre-heated RTM6 and EP2400 resin systems were infiltrated during 1.5-2 hours before heating up to curing temperature of 180 °C and curing for 2 hours. The final parts shown in Fig. 3f were then cut and milled to specimens of size 150 mm x 240 mm x 188 mm. 11 mm holes were drilled and chamfered for load introduction purposes. The final specimens are shown in Fig. 4. Ultrasonic C-scans were performed in order to verify the quality of the specimens and to check for pores or delaminations or other manufacturing-induced pre-damage. Furthermore, micrographs were taken to assess the quality of the fillet and pin reinforcement areas (Fig. 5).

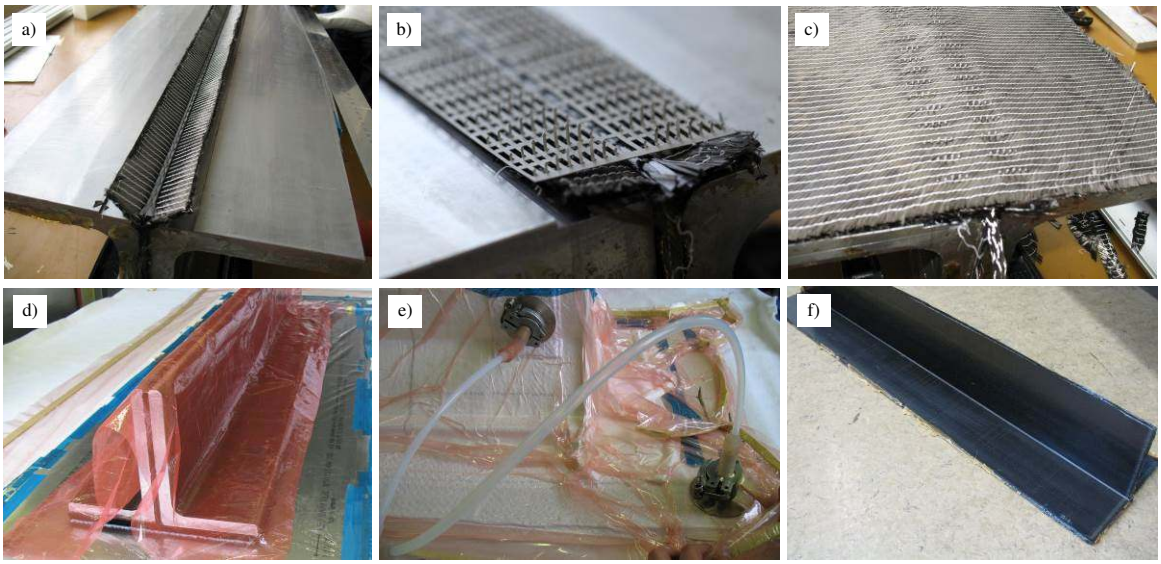

Figure 3: Manufacturing steps of composite T-joints samples: a) placement and cutting of flange plies, b) placement of fillet and metal pin sheet, c) placement of skin laminate, d) preparation for resin injection, e) vacuum-assisted resin injection process, f) final part for eight T-joint samples

© IDMEC 2013

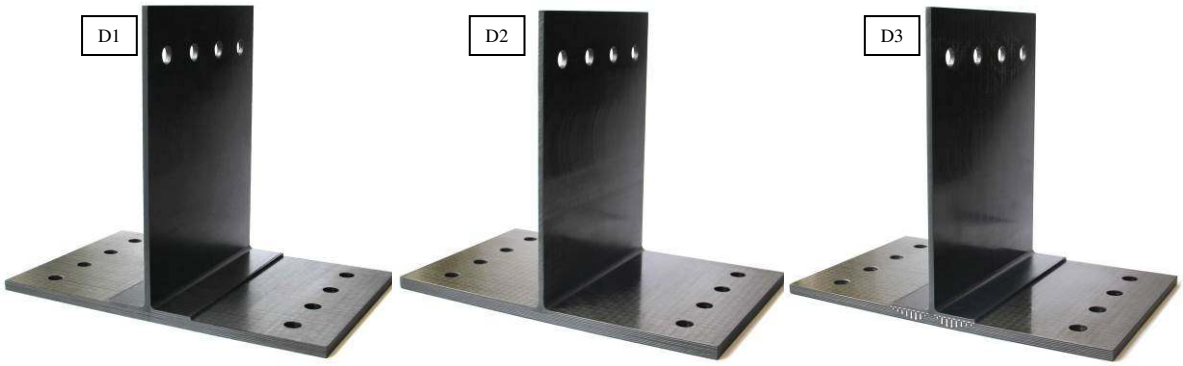

Figure 4: Overview of samples of three composite T-joint designs

Figure 5: Micrographs of D3 specimen: The dark spots are no pores but small resin nests resulting from the non-crimped fabric architecture and the fixation yarns

4. TESTING

The testing campaign of the T-piece specimens was divided into 0° tensile tests (T-pull) and 30° tensile tests (T-bend). While the 0° T-pull loading is a classical simplified test in order to characterise the failure behaviour under pure tension and to compare it to available data in the literature [21], the 30° bending load was regarded as being a more realistic loading scenario for many applications. For example, hydrodynamic ram loads in a fuel-filled wing tank from a penetrating projectile will lead to a pressure wave bending the tank walls and loading the T-joints under bending and tension, which is better represented by a 30° bending/tensile test than by a pure 0° tensile test. T-bend tests under different angles up to 90° have also been performed in [26, 28, 55-57]. The skin part of the T-joint test specimens was clamped at the lateral positions using the boreholes mentioned before.

The tests were performed both with a quasi-static loading rate of 2 mm/min and a high-speed loading rate of 5 m/s in order to assess potential rate effects. The quasi-static tests were performed on a 1000 kN Instron universal testing machine (Fig. 6a) using Aramis optical deformation measurement of the specimen side surface, four to eight strain gauges per specimen on the skin and flange surface and a displacement sensor on the lower skin surface. The dynamic tests were performed on a servo-hydraulic Instron 8503 testing machine (Fig. 6b) with a 60 kN load cell, Aramis optical deformation measurement of the specimen front surface, four strain gauges on the skin and flange surface and two high-speed cameras. At least five specimens were tested for each configuration (design, angle, velocity) with 120 specimens in total.

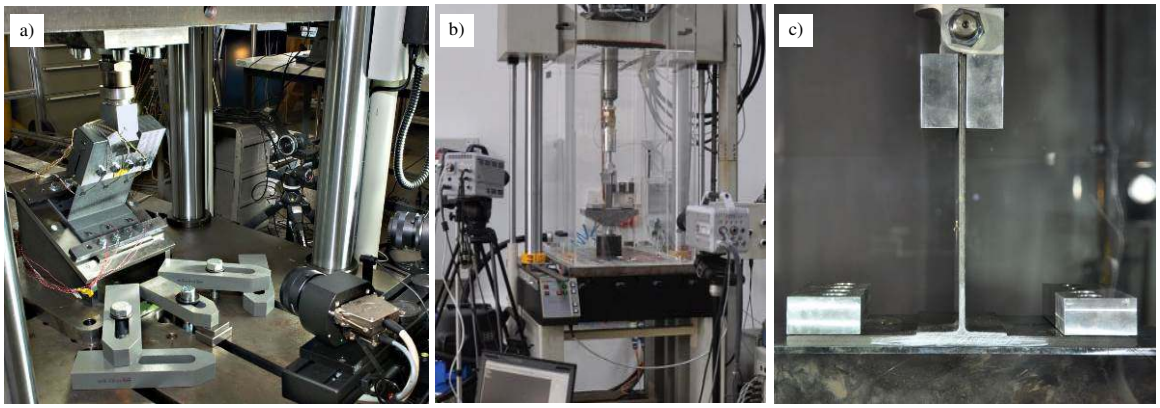

Figure 6: Test set-up: a) quasi-static tests (30° test shown here), b) high-rate dynamic test machine and c) specimen fixation (0° test shown here)

The deformation sequence of all three T-joint designs under quasi-static loading is shown in Fig. 7. The corresponding force-displacement curves of a representative specimen are illustrated in Fig. 8. The D1 specimens fail with a crack initiated in the fillet area in the centre of the specimen, propagating sideward under the flange feet and upwards into the flange. The fillet may stick to the skin or to the flange, both options occurred. Once the crack propagation reaches the end of the flange feet, the flange detaches and the force drops to zero. This failure behaviour corresponds to results of other test campaigns in [12-20].

For D2a specimens with the integral flange feet, the crack initiation is similar in terms of location, peak load and crack propagation. However, as the flange feet are an integral part of the skin with no specific end, the upper plies of the skin are lifted under a higher residual force level and up to much larger displacements. In fact, the test was stopped when the crack propagation reached the clamping supports, without final failure of the specimen. Speaking in terms of application in a composite wing box, structural integrity and leak tightness would still be assured, in contrast to D1.

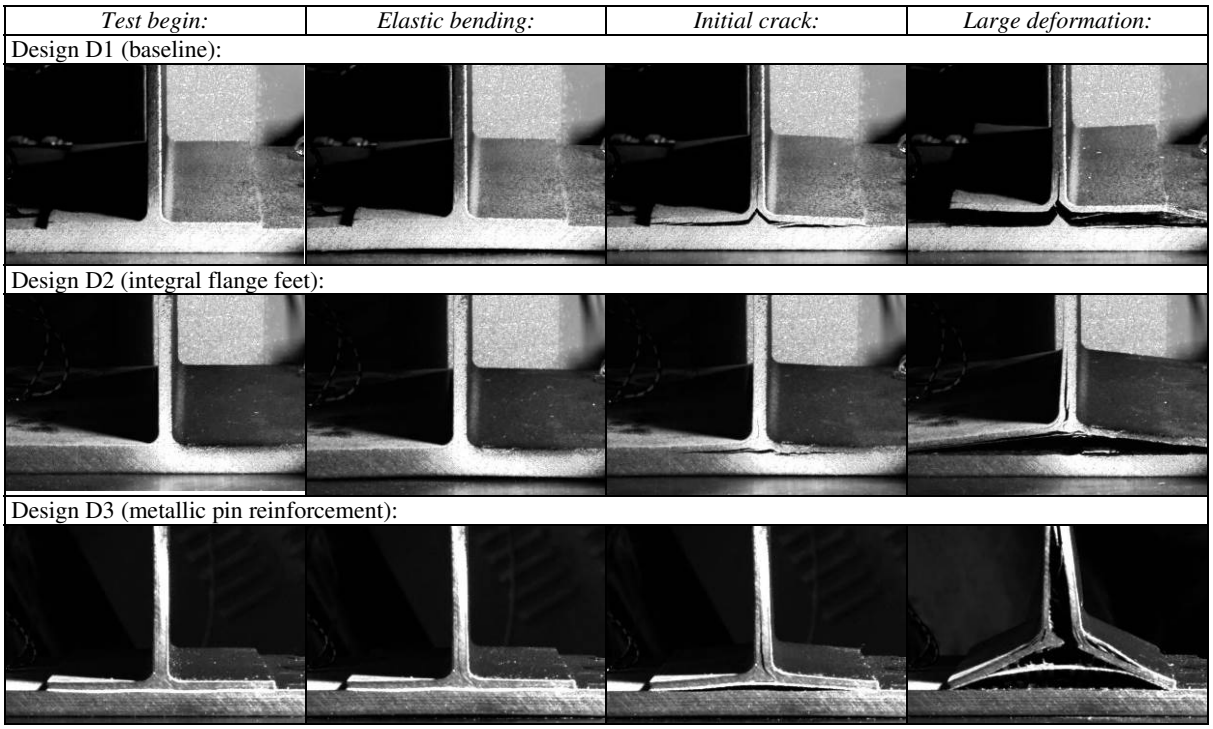

Figure 7: Deformation and failure sequence of all three T-joint designs under quasi-static loading

© IDMEC 2013

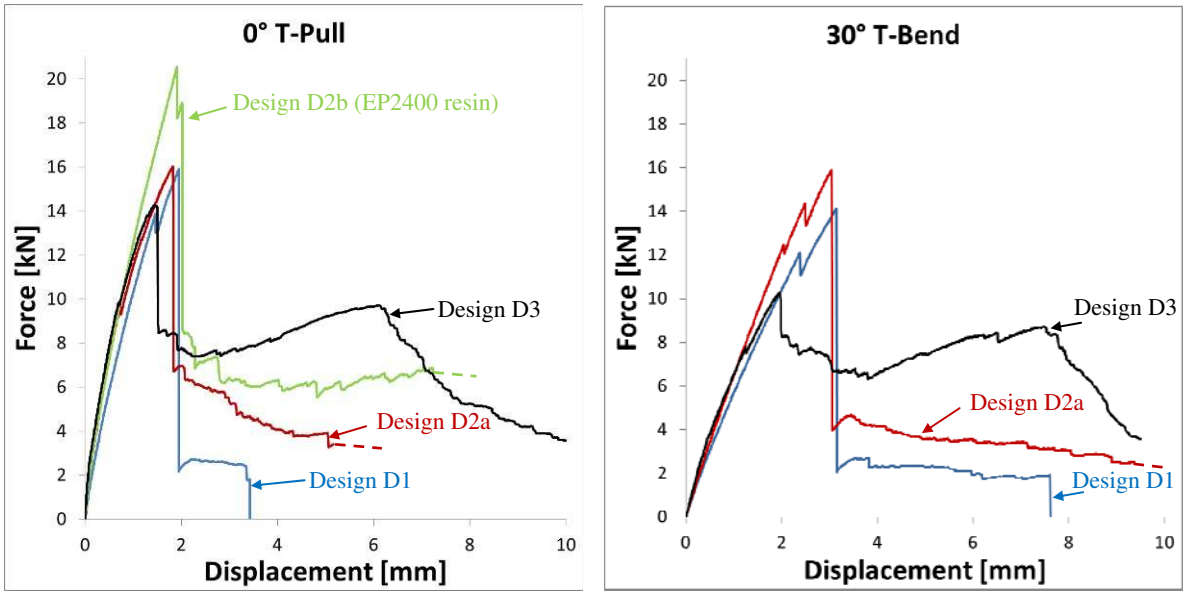

Figure 8: Force-displacement curves of quasi-static T-joint tensile tests under 0° and 30°

Interesting is the result of D2b, where the toughened epoxy resin EP2400 was used instead of RTM6 as in all other specimens. The peak force and also the residual force level after initial failure are significantly higher, about 30%. This corresponds to a much higher energy needed to destroy the structural joint.

Finally, the D3 specimens with a metallic sheet with z-reinforcement pins between skin and flange fail under a slightly lower peak force at the interface between CFRP and metal in the centre of the T-joint. This is because no reinforcement pins were used in the specimen centre in the fillet area that would have significantly improved the performance and that are a preferred option for further specimen manufacturing. Nevertheless, the D3 specimens show their advantages and superior performance in the post-damage behaviour, when the metallic pins are either pulled out of the (upper) laminate or are loaded under tension until they fail. The residual force level is significantly higher than for all other specimens. Complete detachment occurs after very large displacements.

The results of the dynamic T-pull tests with a loading rate of 5 m/s are shown in the force-displacement diagrams in Fig. 9. The force value was derived as $F = E \cdot \varepsilon \cdot A$ from the strain gauge

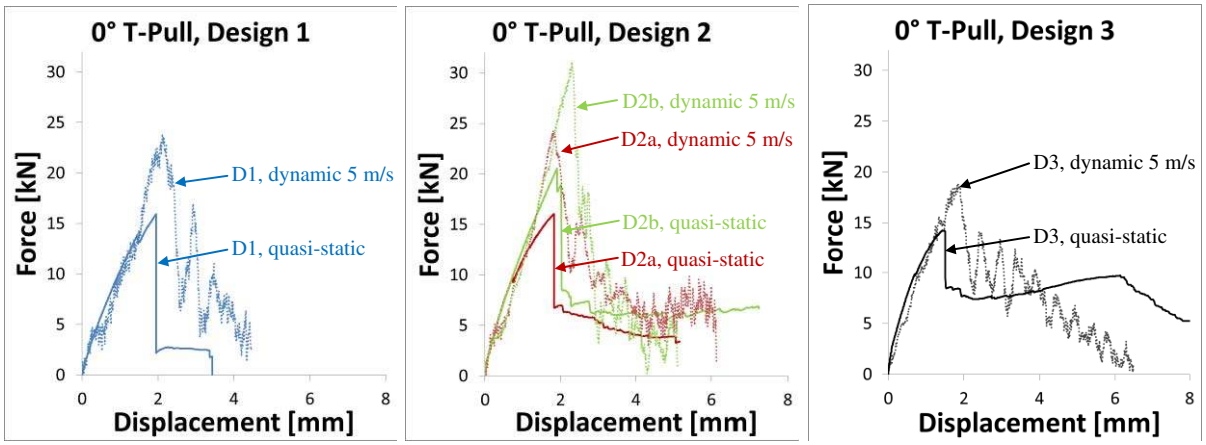

Figure 9: Force-displacement curves of quasi-static and high-rate dynamic 0° T-pull tests

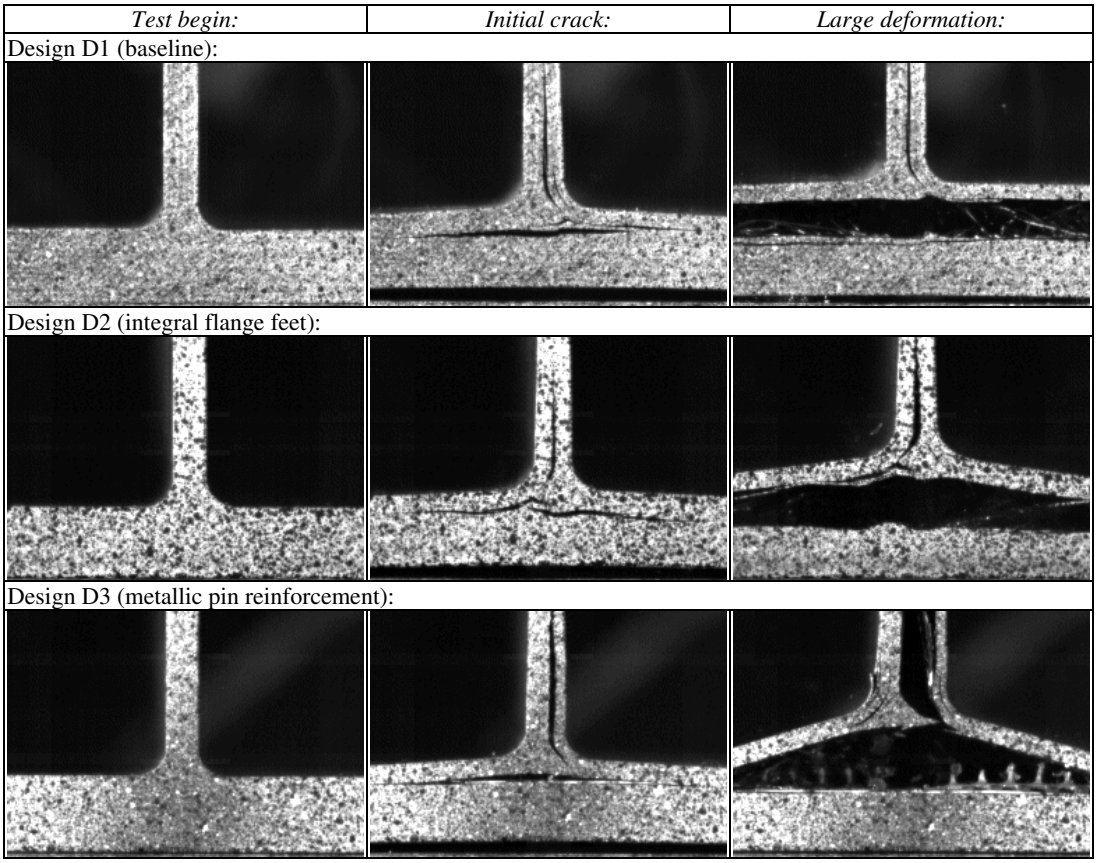

Figure 10: Deformation and failure sequence of three T-joint designs under 0° T-pull dynamic loading (5 m/s) taken from high speed videos

measurements ε on the vertical flange, the flange cross-sectional area A and the effective laminate stiffness E calculated with classical laminate theory. The force values obtained directly from the load cell were too much influenced by inertial effects and could not be used here. In spite of oscillations affecting the force curves resulting from the high-rate dynamic nature of the test, a peak force increase can be observed in Fig. 9 for all three designs. The mode of damage, however, appears to be unchanged. This can be seen in Fig. 10, showing high-speed video images of the T-joint centre area under 0° tension. The crack initiation in the surfaces below and above the fillet as well as the crack propagation pattern appear to be similar to the quasi-static test results.

Summarising the experimental findings, the following lessons were learned:

- An integral design of flange and skin does not improve initial strength but residual strength, energy absorption, structural integrity and leak tightness.
- Using a toughened instead of an untoughened epoxy resin can increase both initial and residual strength significantly.
- The metallic pin reinforcement significantly increases the residual strength and total energy absorption at complete joint failure.
- Rate effects in dynamic tests could be observed, leading to an increase in failure load.

Combining the beneficial options (toughened resin, integral design, pin-reinforcement) in one design would probably lead to superior results.

© IDMEC 2013

5. MODELLING AND SIMULATION

In parallel to the experimental test campaigns numerical simulations with the explicit finite element code LS-DYNA were conducted in order to assess if the mechanical performance obtained in the tests could also be predicted by numerical models and, furthermore, to efficiently investigate further geometrical and boundary influences on the structural behaviour. The models were developed on three different scales: micro, meso and macro scale.

5.1 Micro-scale model

The micro-scale model of the D3 specimen covers a detailed representation of the metallic reinforcement pins and surrounding laminate with solid elements. The aim was to capture the mechanisms of the pins being pulled out of the laminate. All composite parts were modelled with 8-node solid elements with reduced integration and MAT59 (*Mat_Composite_Failure_Solid_ Model), which is a linear elastic, perfect plastic material law with stress-based failure criteria. Element erosion was controlled by the additional implementation of *Mat_Add_Erosion.

Delamination between all plies was enabled by the utilisation of interlaminar contact interfaces (*Contact_Automatic_Surface_to_Surface_Tiebreak) based on the cohesive zone model for mode I and mode II loading. The delamination model was calibrated and validated in advance using double cantilever beam (DCB) and end notch flexure (ENF) tests of the material involved in this study and correlating simulations. The metal pins were modelled using MAT24 (*Mat_Piecewise_Linear_ Plasticity) with elasticity and plasticity parameters for cold-rolled low carbon steel. The model depth was reduced from 150 mm to 30 mm to limit the model complexity but still to cover two rows of upper and lower pins, respectively (Fig. 11). Similar tiebreak contact interfaces were used for the bonding connection of steel and composite with the parameters being based on experimental studies of steel pin pull-out tests in [50, 51].

The final model consisted of 930,000 elements and was very complex due to the high number of nodes and contact interfaces involved. However, despite the high number of simplifications and uncertainties in the model, the simulation results were in fair agreement with the test results, both qualitatively and quantitatively (Fig. 12). The pins were partly pulled out of the laminate with the head partly being intact or sheared off, and some pins were completely torn off (Fig. 13). Major differences between test and simulation mainly occurred at the end of the test after large deformations and massive specimen damage.

This study highlights the potential of such micro-scale models, which can be extended to the investigation of different designs or reinforcement patterns. However, since the efforts in terms of model generation and calculation are immense, they are currently only suitable for specific design investigations and not for an automatic optimisation of the reinforcement architecture.

The micro-scale approach with solid elements for each ply was also extended to study D1 and D2 specimens without z-reinforcement under quasi-static and dynamic loads (Fig. 14, Fig. 15).

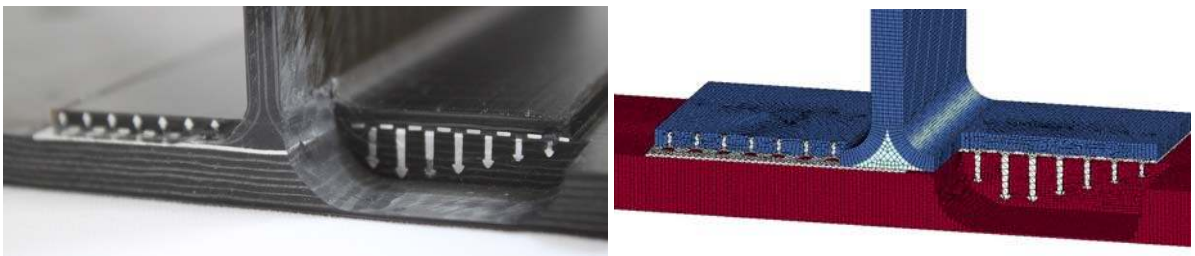

Figure 11: Cross-sectional (milled) view of D3 specimen with metal pin reinforcement and corresponding micro-scale model in LS-DYNA (mesh size 0.5 mm)

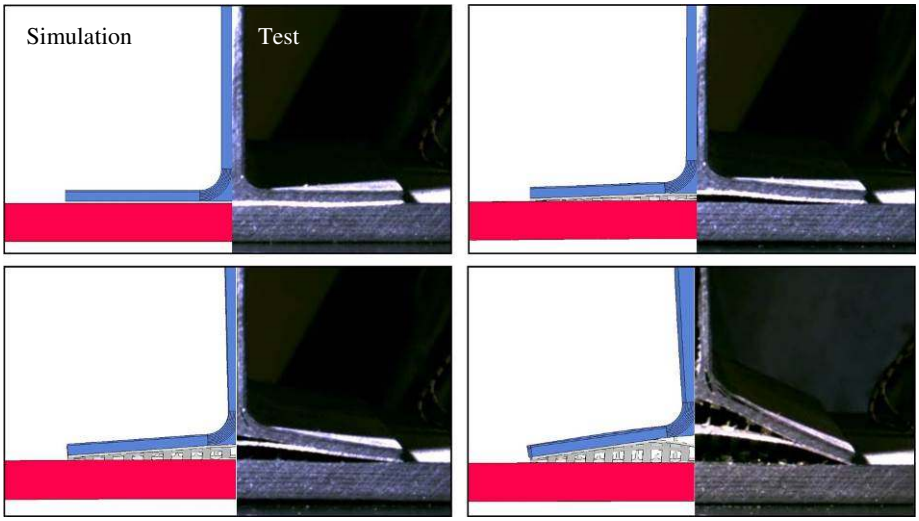

Figure 12: Deformation plots of D3 T-joint in simulation (micro-scale model) and test

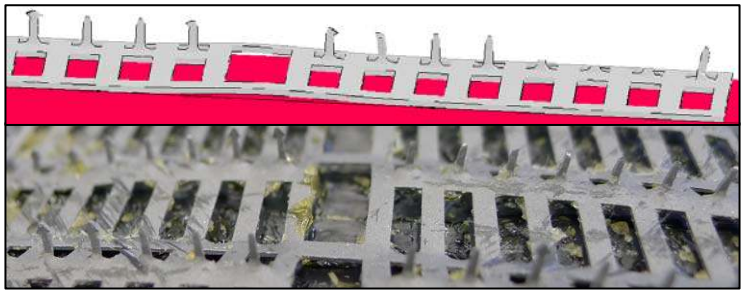

Figure 13: Post-test view of failed pins in micro-scale simulation and test

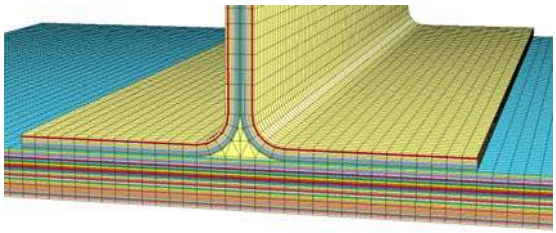

Figure 14: Micro-scale model of D1 specimen (mesh size 2 mm)

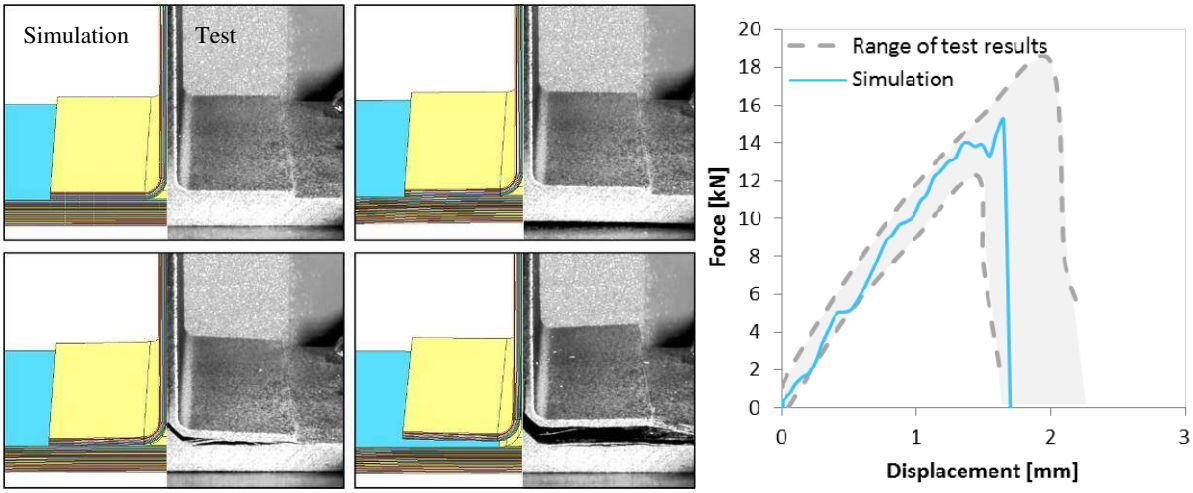

Figure 15: Comparison of quasi-static tensile test and simulation (micro-scale model) of D1 T-joint: deformation plots (left) and force-displacement curves (right)

© IDMEC 2013

5.2 Meso-scale model

The meso-scale models are a major simplification and only consist of 4-node shell elements with reduced integration for the skin and flange. Only the fillet is modelled with solid elements (Fig. 16). According to the experimental observations in Fig. 7 and Fig. 10, delamination contact interfaces (*Contact_Automatic_Surface_to_Surface_Tiebreak) were only used between the skin and flange (and fillet) and within the flange itself. MAT54 (*Mat_Enhanced_Composite_Damage) was used for the composite material modelling, which is an orthotropic, linear elastic, perfect plastic constitutive law with stress-based failure criteria and strain-based element erosion.

The simulation results of D2 are shown in Fig. 17 as an example of the meso models. The failure behaviour with delaminations developing between skin and flange as well as within the flange is captured well and the force-displacement response correlates well with the experiments. Only the residual strength in the post-damage region is underestimated in this example.

The number of elements and CPU time of this model are much lower compared to the micro-modelling approach, but the results accuracy is similar. This is due to the fact that only this limited number of delamination interfaces is necessary to represent realistic failure behaviour, and solid elements are not necessary since this is a bending-dominated problem and the out-of-plane stresses do not necessarily need to be implemented, making the shell modelling approach the more efficient solution.

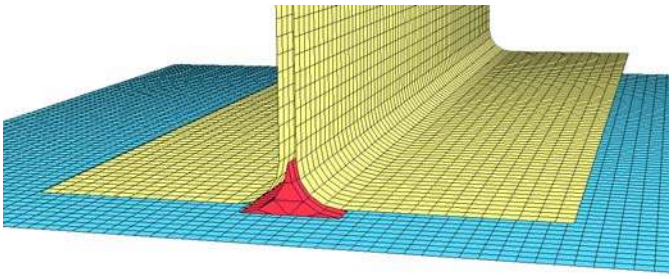

Figure 16: Meso-scale model of D1 specimen (mesh size 2 mm)

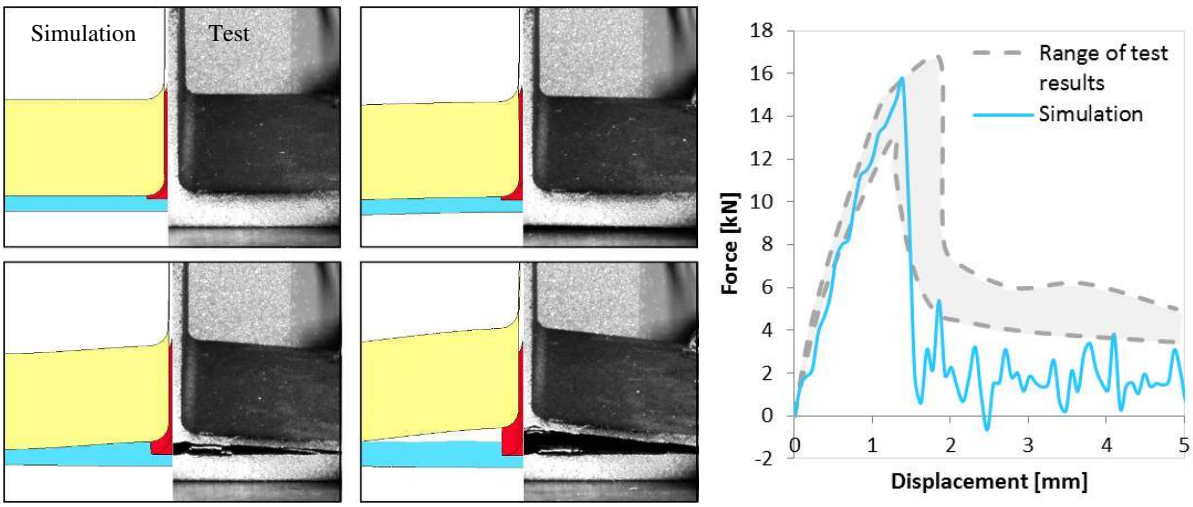

Figure 17: Comparison of quasi-static tensile test and simulation (meso-scale model) of D2 T-joint: deformation plots (left) and force-displacement curves (right)

5.3 Macro-scale model

The intention for investigating T-joint models on the macro scale was to use them in large wing or wing box models, where it would not be possible to implement the still too detailed meso-scale models. Much simpler and coarser models are needed for this kind of application, which should still be able to represent the global failure behaviour of the T-joint designs in terms of failure initiation and nonlinear post-failure behaviour.

Different options in LS-DYNA exist that could theoretically be used to represent the structural joint on macro level. These are mainly contact algorithms, nodal constraints or special element and material formulations. In general, the method of choice should be able to meet the following six requirements:

1. Transfer moments between flange and skin, separation of normal and shear behaviour;
2. Failure of the connection should be covered
3. Post-failure behaviour should be covered (nonlinear, correct residual force level and energy absorption)
4. Separation of the joined partners needs to be implemented beyond failure
5. Strain rate effects need to be covered
6. Simple approach: minor modelling and calculation efforts.

Since the contact laws cannot fulfil most of these requirements and also the constraints lack in post-damage behaviour and strain rate effects, the focus was put on representing the joint behaviour in a specific row of elements in the connection zone with an appropriate material model.

Finally, shell elements with MAT123 (*Mat_Modified_Piecewise_Linear_Plasticity_Rate) were used, as this approach covers all six of the abovementioned requirements. The user has to define the elastic stiffness *E*, which represents the homogenised stiffness of the composite flange laminate, the yield stress *SIGY*, the nonlinear post-damage behaviour *LCSS* as tabular input of stress vs. plastic strain and the plastic strain at failure *FAIL* (Fig. 18). The latter three inputs were derived and calibrated in accordance with the test results in Fig. 8. Strain rate effects can be incorporated by a simple Cowper-Symonds yield stress scaling law, by a tabular yield stress scaling law, by tabular input of the stress-strain curve for different strain rates and by tabular input of strain at failure as a function of strain rate.

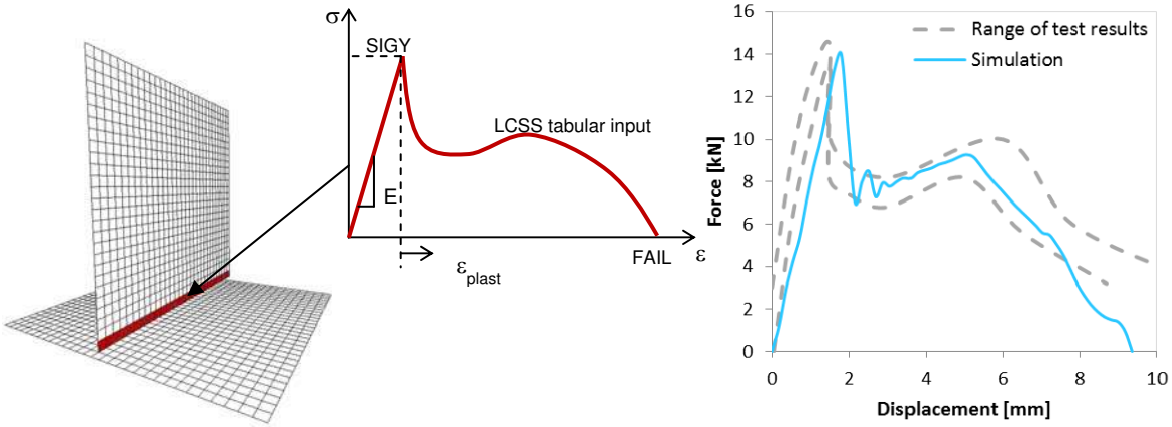

Figure 18: Macro-scale model with homogenised, generic input data for joint failure representation (left) and global force-displacement response of D3 macro model (right)

© IDMEC 2013

The model behaviour was validated in 0° and 30° tensile test simulations of the T-joint, which required more than 90% less CPU time than the comparable meso models and were finished after a few seconds. The global T-joint failure behaviour was represented with a high degree of accuracy, making this model applicable in large wing box analyses.

5.4 Application to hydrodynamic ram simulation of fuel-filled wing tank

The application of the models developed here to the ballistic impact and hydrodynamic ram (HRAM) analysis of a fuel-filled composite wing tank box shall shortly be addressed. The aim was to assess the mechanical performance of the three different T-joint designs in a large structural assembly under HRAM loads.

The structures were generic composite boxes in a 3-cell and 12-cell configuration, representing military aircraft wing segments (Fig. 19, Fig. 20). These structures were developed, built and used for ballistic impact tests with the focus on the HRAM behaviour in the past project EUCLID RTP 3.32 [58]. The models of the 3- and 12-cell wing box were generated in LS-DYNA using the T-joint macro models and the Arbitrary Lagrangian-Eulerian (ALE) approach to model the fluid filling and fluid-structure interaction. Simulating HRAM in fuel tanks with LS-DYNA and ALE is state of the art and has also been performed in numerous studies like in [1-3, 59-62]. The projectile was a 4.7 g steel cylinder, modelled as a rigid body, with an initial velocity of 1600 m/s. Test data of the previous project [58] in terms of pressure sensor measurements inside the fuel-filled box and post-test damage assessment were used to validate the simulations.

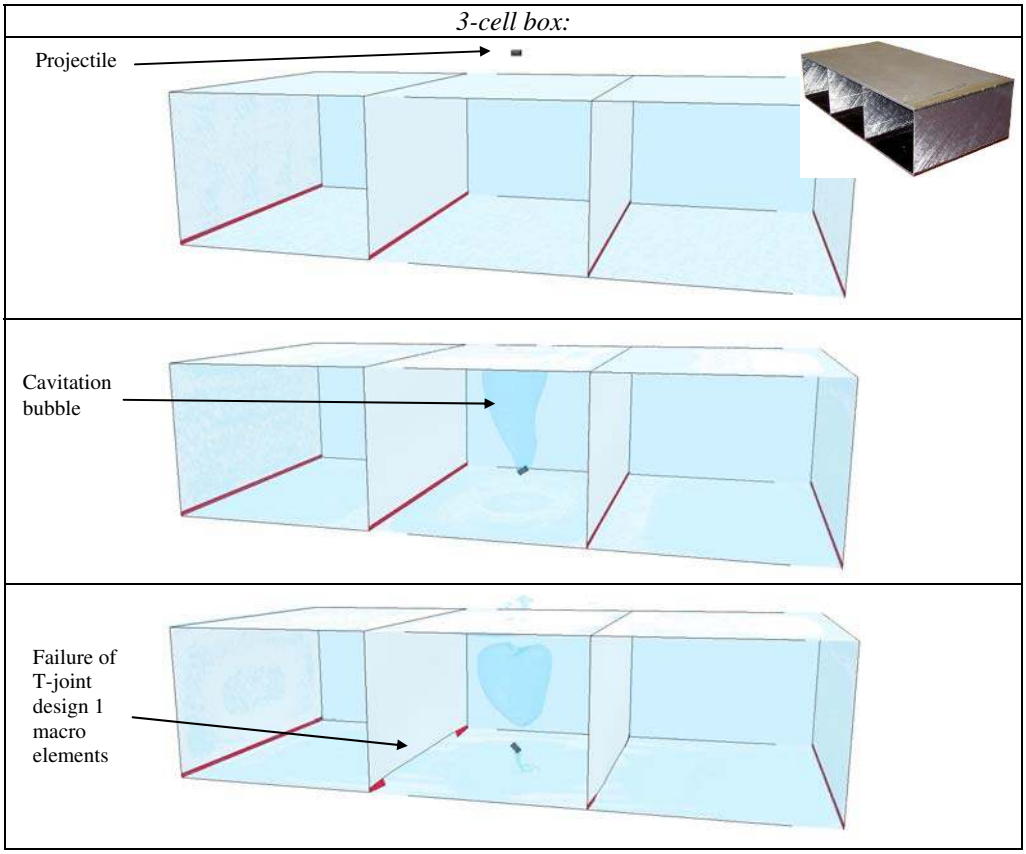

Figure 19: Ballistic impact and hydrodynamic ram simulation of fluid-filled composite 3-cell box according to [58]: Failure of D1 T-joint macro elements

The simulations were used to assess the structural performance of the three T-joint designs under this hydrodynamic ram load. After penetration of the front skin, a high pressure shock wave is formed and propagates through the fluid with a short-time peak loading of the structure. Afterwards, the projectile is intruding and pushes the fluid aside, leading to a further structural loading with a longer duration. The T-joints of design D1 fail under this load, while design D2 and D3 are still intact. This is in accordance with the experimental findings and supports the performance enhancements by the integral design, improved resin system and z-reinforcement. The failure of D1 macro elements in the 3-cell box is visualised in Fig. 19 and in the 12-cell box in Fig. 20. Both show a translucent view of a ballistic impact simulation with the coloured macro elements being eroded under the high pressure load.

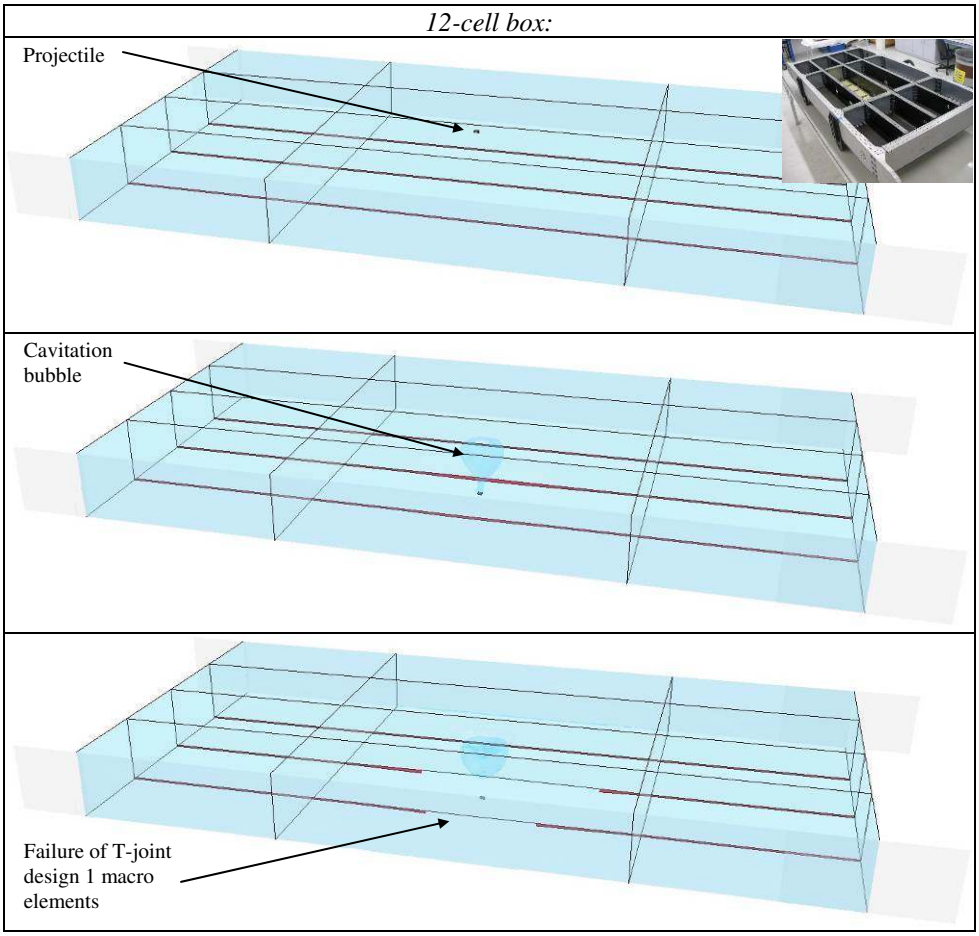

Figure 20: Ballistic impact and hydrodynamic ram simulation of fluid-filled composite 12-cell box according to [58]: Failure of D1 T-joint macro elements

6. CONCLUSIONS

Three different composite T-joint designs were investigated experimentally and numerically under 0° and 30° tensile loads and under quasi-static and dynamic loading rates. The unreinforced baseline design D1 showed a rather brittle behaviour and failed early in the hydrodynamic ram simulation of a fuel-filled wing tank under ballistic impact. An advanced toughened resin system in combination with an integral design D2 led to significant improvements in terms of initial and residual strength increase and structural integrity in the reference HRAM load case. This result was also obtained for the hybrid design D3 with metallic, arrow-shaped z-reinforcements, which showed the best residual strength behaviour.

© IDMEC 2013

Modelling and simulation studies of the composite T-joints were performed on micro, meso and macro level. While the modelling efforts on micro level are relatively expensive, the more efficient meso models showed promising results in good correlation to the experimental findings. Delamination modelling with adequate cohesive interfaces and accurate parameter selection appears to be the major factor for realistic simulation results. A promising macro modelling approach for an efficient representation of the T-joint failure behaviour in large models was derived and successfully applied to structural HRAM simulations.

ACKNOWLEDGEMENTS

This investigation was performed in the framework of the contract E/E210/AB005/BF114 “Festigkeitssteigerung von strukturellen Verbindungen in Integraltanks unter hydrodynamischen Lasten” with public funding by the German Federal Ministry of Defence. The financial support is gratefully acknowledged.

References

[1] C. Less, S. Hauck, N. Langhans, R. Polis, P. Middendorf, P. Stephani, W. Riedel, V. Schacht, MALE UAV vulnerability. ESW2006 - 3rd European Survivability Workshop, Toulouse, 2006.
[2] P. Stephani, P. Middendorf, C. Less, Numerical analysis of the hydrodynamic ram of a CFRP integral tank. Structures Under Shock and Impact IX, N. Jones (ed), 2006, WIT Press, pp. 45-55.
[3] D. Varas, R. Zaera, J. Lopez-Puente, Numerical modelling of partially filled aircraft fuel tanks submitted to hydrodynamic ram. Aerospace Science and Technology, 16, 2012, 19-28.
[4] R. Vignjevic, T. De Vuyst, J. Campbell, N. Bourne, Modelling of impact on a fuel tank using smoothed particle hydrodynamics. 5th International Conference on Dynamics and Control of Systems and Structures in Space, Cambridge, UK, 2002.
[5] P. Santini, D. Palmieri, M. Marchetti, Numerical simulation of fluid-structure interaction in aircraft fuel tanks subjected to hydrodynamic ram penetration. 21st ICAS, Melbourne, 1998.
[6] T. Wierzbicki, N.A. Moussa, Deformation and rupture of an aircraft fuel tank under hydraulic ram pressure loading. 63rd Shock and Vibration Symposium, Las Cruces, NM, 1992.
[7] E.A. Lundstrom, Fuel cell structural response to hydraulic ram. PVP-Vol. 134, Shock and Wave Propagation, ASME, 1988, pp. 39-51.
[8] C.H.M. Helwig, G.W. Sachs, K.G.K. Seidel, Numerical investigation of hydraulic ram effects in fuel tanks. 10th International Symposium on Ballistics, San Diego, CA, 1987.
[9] M.A. Ferman, W.H. Unger, Fluid-structure interaction dynamics in aircraft fuel tanks. Journal of Aircraft, 16, 1979, 885-890.
[10] M. Lee, R.G. Longoria, D.E. Wilson, An extended hydraulic ram model. PVP-Vol. 325, Structures Under Extreme Loading Conditions, ASME, 1996, pp. 75-82.
[11] C.M. Seddon, K. Moodie, A.M. Thyer, M. Moatamedi, Preliminary analysis of fuel tank impact. International Journal of Crashworthiness, 9, 2004, 237-244.
[12] T. Yang, J. Zhang, A.P. Mouritz, C.H. Wang, Healing of carbon fibre-epoxy composite T-joints using mendable polymer fibre stitching. Composites Part B, 45, 2013, 1499-1507.
[13] F. Bianchi, T.M. Koh, X. Zhang, I.K. Partridge, A.P. Mouritz, Finite element modelling of z-pinned composite T-joints. Composites Science and Technology, 73, 2012, 48-56.
[14] R.S. Trask, S.R. Hallett, F.M.M. Helenon, M.R. Wisnom, Influence of process induced defects on the failure of composite T-joint specimens. Composites Part A, 43, 2012, 748-757.
[15] T.M. Koh, S. Feih, A.P. Mouritz, Experimental determination of the structural properties and strengthening mechanisms of z-pinned composite T-joints. Comp. Struct., 93, 2011, 2222-2230.
[16] G.A.O. Davies, J. Ankersen, Virtual testing of realistic aerospace composite structures. Journal of Materials Science, 43, 2008, 6586-6592.
[17] K. Vijayaraju, P.D. Mangalgiri, B. Dattaguru, Experimental study of failure and failure

progression in T-stiffened skins. Composite Structures, 64, 2004, 227-234.
[18] J. Li, J.K. Sen, Analysis of frame-to-skin joint pull-off tests and prediction of the delamination failure. 42nd AIAA/ASME/ASCE/AHS/ASC Structures, Structural Dynamics and Materials Conference, Seattle, WA, 2001.
[19] P.L. LeBoulluec, W.S. Chan, M.G. Filips, Stiffener attachment of composite structures. Durability of Composite Materials, MD-Vol. 51, ASME Winter Meeting, 1994, pp. 147-158.
[20] R.I. Haresceugh, G.W. Rogers, C. Shaw, D.H. Woolstencroft, Development of an advanced technology wing. In: Middelton, D.H. (ed.), Composite Materials in Aircraft Structures. Longman Scientific & Technical, 1990, pp. 249-259.
[21] M. Herkt, P. Middendorf, C. Less, W. Riedel, G. Maier, K. Drechsler, Dynamic strength testing of 3D-reinforced T-joints. 25th ICAS Congress, Hamburg, 2006.
[22] S.P. Renze, S.W. Carnegie, F. Sandow, Experimental evaluation of survivable composite structural concepts. 37th AIAA/ASME/ASCE/AHS/ASC Structures, Structural Dynamics and Materials Conference and Exhibit, Salt Lake City, UT, 1996, 39-46.
[23] M.A. Moshier, R.L. Hinrichsen, G.J. Czarnecki, N.L. Cook, Testing composite joints under high energy hydrodynamic ram conditions. 45th AIAA/ASME/ASCE/AHS/ASC Structures, Structural Dynamics & Materials Conference, Palm Springs, CA, 2004.
[24] G.J. Czarnecki, R. Hinrichsen, M. Maxson, Joint resistance to ram. U.S. Air Force T&E Days, Nashville, TN, 2005.
[25] G.J. Czarnecki, R. Hinrichsen, Assessment of dynamic skin-spar joint failure properties. U.S. Air Force T&E Days, Destin, FL, 2007.
[26] J. Chen, D. Fox, Numerical investigation into multi-delamination failure of composite T-piece specimens under mixed mode loading using a modified cohesive model. Composite Structures, 94, 2012, 2010-2016.
[27] F. Helenon, M.R. Wisnom, S.R. Hallett, R.S. Trask, Numerical investigation into failure of laminated composite T-piece specimens under tensile loading. Composites Part A, 43, 2012, 1017-1027.
[28] L.A. Burns, A.P. Mouritz, S. Feih, Application of a bio-inspired design strategy to delay damage initiation in a FRP T-joint under bending. ICCM18, Jeju, Korea, 2011.
[29] J. Chen, E. Ravey, S. Hallett, M. Wisnom, M. Grassi, Prediction of delamination in braided composite T-piece specimens. Composites Science & Technology, 69, 2009, 2363-2367.
[30] S.K. Panigrahi, B. Pradhan, Delamination damage analyses of FRP composite spar wingskin joints with modified elliptical adhesive load coupler profile. Appl. Compos. Mater., 15, 2008, 189-205.
[31] G.A.O. Davies, D. Hitchings, J. Ankersen, Predicting delamination and debonding in modern aerospace composite structures. Composites Science & Technology, 66, 2006, 846-854.
[32] K.N. Mune Gowda, A.V. Sunil Kumar, H.S. Vijayakumari, B. Dattaguru, T.S. Ramamurthy, 3-D finite element analysis of T-pull joints in composite wing structures. 12th National Seminar on Aerospace Structures, NASAS XII, Bangalore, 2003.
[33] S. Kumari, P.K. Sinha, Finite element analysis of composite wing T-joints. Journal of Reinforced Plastics and Composites, 21, 2002, 1561-1585.
[34] G.F.J. Hill, M.R. Wisnom, M. Jones, Failure prediction of composite T-piece specimens. 5th International Conference on Deformation and Fracture of Composites, London, 1999.
[35] P.B. Stickler, M. Ramulu, Experimental study of composite T-joints under tensile and shear loading. Advanced Composite Materials, 15, 2006, 193-210.
[36] P.B. Stickler, M. Ramulu, Parametric analyses of stitched composite T-joints by the finite element method. Materials & Design, 23, 2002, 751-758.
[37] P.B. Stickler, M. Ramulu, P.S. Johnson, Experimental and numerical analysis of transverse stitched T-joints in bending. Composite Structures, 50, 2000, 17-27.
[38] V.V.S. Rao, K. Krishna Veni, P.K. Sinha, Behaviour of composite wing T-joints in hygrothermal environments. Aircraft Engineering & Aerospace Technology, 76, 2004, 404-413.
[39] S. Kumari, P.K. Sinha, Effects of transverse stitching and hygrothermal environment on composite wing T-joints. Journal of Reinforced Plastics and Composites, 22, 2003, 1705-1728.

© IDMEC 2013

[40] J. Li, Pull-off tests and analyses of composite skin and frame T-joint. 17th Annual ASC Technical Conference on Composite Materials, West Lafayette, IN, 2002.
[41] W.B. Young, M.T. Chuang, Fabrication of T-shaped structural composite through resin transfer molding. Journal of Composite Materials, 29, 1995, 2192-2214.
[42] Y. Tada, T. Ishikawa, Experimental evaluation of the effects of stitching on CFRP laminate specimens with various shapes and loadings. Key Engineering Materials, 37, 1989, 305-316.
[43] D.D.R. Cartie, G. Dell'Anno, E. Poulin, I.K. Partridge, 3D reinforcement of stiffener-to-skin T-joints by z-pinning and tufting. Engineering Fracture Mechanics, 73, 2006, 2532-2540.
[44] T.M. Koh, S. Feih, A.P. Mouritz, Strengthening mechanics of thin and thick composite T-joints reinforced with z-pins. Composites Part A, 43, 2012, 1308-1317.
[45] Y.B. Park, B.H. Lee, J.H. Kweon, J.H. Choi, I.H. Choi, The strength of composite bonded T-joints transversely reinforced by carbon pins. Composite Structures, 94, 2012, 625-634.
[46] G. Allegri, X. Zhang, On the delamination and debond suppression in structural joints by z-fibre pinning. Composites Part A, 38, 2007, 1107-1115.
[47] J. Meyer, A revolution in hybrid component manufacture. SETEC 09 – SAMPE Europe Technical Conference, Filton/Bristol, UK, 2009.
[48] D.P. Graham, A. Rezai, D. Baker, P.A. Smith, J.F. Watts, A hybrid joining scheme for high strength multi-material joints. ICCM18 – 18th Int. Conf. on Composite Materials, Jeju, 2011.
[49] S. Ucsnik, M. Scheerer, S. Zaremba, D.H. Pahr, Experimental investigation of a novel hybrid metal-composite joining technology. Composites Part A, 41, 2010, 369-374.
[50] A.C. Nogueira, K. Drechsler, E. Hombergsmeier, M. Pacchione, Investigation of the properties and failure mechanisms of a damage tolerant 3D-reinforced joint for lightweight structures. ICCS16 – 16th International Conference on Composite Structures, Porto, 2011.
[51] H. Lang, A.C. Nogueira, K. Drechsler, E. Hombergsmeier, Development and optimization of an innovative joining technique for composite structures using the finite element method. ECCOMAS 2013, Vienna, 2012.
[52] A.C. Nogueira, K. Drechsler, E. Hombergsmeier, Analysis of the static and fatigue strength of a damage tolerant 3D-reinforced joining technology on composite single lap joints. 53rd AIAA/ASME/ASCE/AHS/ASC Structures, Struct. Dynamics and Mat. Conf., Honolulu, 2012.
[53] A.R. Rispler, G.P. Steven, L. Tong, Failure analysis of composite T-joints including inserts. Journal of Reinforced Plastics and Composites, 16, 1997, 1642-1658.
[54] R.D. Cope, R.B. Pipes, Design of the spar-wingskin joint. 4th Conference on Fibrous Composite in Structural Design, San Diego, CA, 1978, pp. 603-617.
[55] H.J. Phillips, R.A. Shenoi, Damage tolerance of laminated tee joints in FRP structures. Composites Part A, 29, 1998, 465-478.
[56] G.L. Hawkins, R.A. Shenoi, A parametric study to determine the influence of geometric variations on the performance of a bulkhead to shell plating joint. ICCM9 – 9th International Conference on Composite Materials, Madrid, 1993, pp. 97-104.
[57] R.A. Shenoi, G.L. Hawkins, Influence of material and geometry variations on the behaviour of bonded tee connections in FRP ships. Composites, 23, 1992, 335-345.
[58] EUCLID RTP 3.32 Low vulnerablity composite structures for military aircraft, Synthesis report RTP-3.32/7/TR/EADS-D/045/D, EADS, Ottobrunn, 2007.
[59] S.C. McCallum, D.D. Townsend, Simulation of hydrodynamic ram and liquid aeration. 5th European LS-DYNA Users Conference, Birmingham, UK, 2005.
[60] F. Poehlmann-Martins, J. Gabrys, M. Souli, Hydrodynamic ram analysis of non-exploding projectile impacting water. ASME Pressure Vessels and Piping Division Conf., Denver, 2005.
[61] C.M. Seddon, M. Moatamedi, Fluid structure interaction of fuel tank impact. 1er Colloque du GDR Interactions Fluide-Structure, Sophia Antipolis, France, 2005.
[62] C.E. Sparks, R.L. Hinrichsen, D. Friedmann, Comparison and validation of smooth particle hydrodynamic (SPH) and coupled Euler Lagrange (CEL) techiques for modeling hydrodynamic ram. 46th AIAA/ASME/ASCE/AHS/ASC Structures, Structural Dynamics & Materials Conference, Austin, TX, 2005.